PNAS RESEARCH ARTICLE | MICROBIOLOGY OPEN ACCESS

N6-methyladenosine modification of a parvovirus-encoded small noncoding RNA facilitates viral DNA replication through recruiting Y-family DNA polymerases

Kang Ning[a], Junxing Zhao[b,c], Zehua Feng[d], Soo Yeun Park[d], Shane McFarlin[a], Fang Cheng[a], Ziying Yan[d], Jingxin Wang[b,c], and Jianming Qiu[a,1]

Affiliations are included on p. 11.

Edited by Michael J. Imperiale, University of Michigan-Ann Arbor, Ann Arbor, MI; received November 27, 2023; accepted May 14, 2024 by Editorial Board Member Xiang-Jin Meng

Human bocavirus 1 (HBoV1) is a human parvovirus that causes lower respiratory tract infections in young children. It contains a single-stranded (ss) DNA genome of ~5.5 kb that encodes a small noncoding RNA of 140 nucleotides known as bocavirus-encoded small RNA (BocaSR), in addition to viral proteins. Here, we determined the secondary structure of BocaSR in vivo by using DMS-MaPseq. Our findings reveal that BocaSR undergoes N6-methyladenosine (m6A) modification at multiple sites, which is critical for viral DNA replication in both dividing HEK293 cells and nondividing cells of the human airway epithelium. Mechanistically, we found that m6A-modified BocaSR serves as a mediator for recruiting Y-family DNA repair DNA polymerase (Pol) η and Pol κ likely through a direct interaction between BocaSR and the viral DNA replication origin at the right terminus of the viral genome. Thus, this report represents direct involvement of a viral small noncoding RNA in viral DNA replication through m6A modification.

m6A modification | viral noncoding RNA | parvovirus | DNA replication

Significance

Human bocavirus 1 (HBoV1), an autonomously replicating human parvovirus, is a human pathogen that causes lower respiratory tract infections in young children. HBoV1 expresses a small noncoding RNA (sncRNA), named bocavirus-encoded small RNA (BocaSR), which is the first reported RNA polymerase (Pol) III–transcribed viral sncRNA in small DNA viruses that do not encode a viral DNA Pol. BocaSR is N6-methyladenosine (m6A)-modified at multiple sites, which mediates BocaSR to recruit two Y-family DNA repair Pols, Pol η and Pol κ, to the viral DNA replication origin (*Ori*) through a direct interaction. Thus, we elucidated a viral DNA replication mechanism, in which a viral sncRNA utilizes m6A modification to direct DNA repair DNA Pols to the viral *Ori* for viral DNA replication.

Human bocavirus 1 (HBoV1) is an emerging human pathogen that affects the lower respiratory tract, especially in children under 5 y old worldwide (1, 2). In infants, severe HBoV1 infection can progress to bronchopneumonia and bronchiolitis, with common clinical symptoms including coughing, wheezing, and fever (1–3). HBoV1 is an autonomously replicating parvovirus, belonging to *Primate bocaparvovirus 1* in the genus *Bocaparvovirus* of the family *Parvoviridae* (4). It consists of a single-stranded DNA (ssDNA) genome of 5,543 nucleotides (nts), which is flanked by two terminal palindromic sequences, the left-end hairpin (LEH) and the right-end hairpin (REH) (5). These hairpin structures contain *cis* signals for viral DNA replication and genome packaging (5, 6). The HBoV1 genome encodes five nonstructural proteins (NS1-4 and NP1) and three structural capsid proteins (VP1, VP2, and VP3). These proteins are expressed from the viral mRNA transcripts that are alternatively spliced and polyadenylated from a single precursor mRNA (pre-mRNA) (7–9). Notably, HBoV1 transcribes a small noncoding RNA (sncRNA) of 140 nt from the noncoding region (NCR) at the 3′ end of the genome, using an intragenic RNA polymerase III (Pol III) (10). This sncRNA was named bocavirus-encoded small RNA (BocaSR). While NS1 and NP1 are essential for viral DNA replication (5, 8, 11), BocaSR also plays a crucial role in viral DNA replication in both dividing human embryonic kidney (HEK) 293 cells transfected with a duplex HBoV1 genome and nondividing cells of the well-differentiated human airway epithelium (HAE) infected with HBoV1 (10).

BocaSR represents the first RNA Pol III–transcribed RNA discovered among small DNA viruses that do not express a viral DNA Pol, including papillomaviruses, polyomaviruses, circoviruses, and parvoviruses (12). It represents a novel RNA Pol III–transcribed virus-encoded sncRNA, alongside the adenovirus (Ad)-associated (VA) RNAs (VA RNAI and VA RNAII) (13) and Epstein–Barr virus (EBV)-encoded small RNAs (EBER1 and EBER2) (14). VA RNAs are transcribed in the nucleus and exported to the cytoplasm (13), where they interact with the dsRNA-activated protein kinase R (PKR) to inhibit PKR activation and subsequent phosphorylation of eukaryotic initiation factor 2 (eIF2α) (15). EBERs are located primarily in the nucleus (16). EBER1 binds to La protein, the ribosomal protein L22, and AU-rich element-binding factor 1 [AUF1/heterogeneous nuclear ribonucleoprotein D (hnRNPD)] (12). EBER2 interacts with nascent transcripts from the terminal repeats (TRs) of the EBV genome and recruits transcription factor PAX5 to the TRs to facilitate EBV lytic replication (17). While the

Author contributions: K.N., Z.Y., J.W., and J.Q. designed research; K.N. and J.Z. performed research; K.N., Z.F., S.Y.P., and F.C. contributed new reagents/analytic tools; K.N., J.Z., and J.W. analyzed data; Z.Y., J.W., and J.Q. provides funds and manages the project; and K.N., J.Z., S.M., Z.Y., J.W., and J.Q. wrote the paper.

Competing interest statement: Z.Y. and J.Q. have submitted a US patent application related to BocaSR (WO2018132747A1).

This article is a PNAS Direct Submission. M.J.I. is a guest editor invited by the Editorial Board.

[1]To whom correspondence may be addressed. Email: jqiu@kumc.edu.

This article contains supporting information online at https://www.pnas.org/lookup/suppl/doi:10.1073/pnas.2320782121/-/DCSupplemental.

Published June 14, 2024.

sequence and putative secondary structure of BocaSR share significant similarity with the VA RNAI, it does not inhibit PKR phosphorylation. Instead, BocaSR more closely resembles the nuclear localization of EBER2 (10).

Modified nucleotides within cellular RNAs were discovered in the 1960s. Up to date, more than 100 known RNA chemical modifications have been identified (18), including N6-methyladenosine (m6A), 5-methylcytosine (m5C), N7-methylguanosine (m7G), 8-Oxoguanine (o8G), and pseudouridine (Ψ) (19–23). These modifications have been proven to be present not only in cellular ncRNAs but also in viral mRNAs, regulating diverse aspects of RNA metabolism (19, 20, 24, 25). Notably, while EBER2 is not modified, EBER1 possesses a m5C modification; however, the m5C modification of EBER1 is not required for viral lytic replication (26). Among these RNA modifications, m6A is the most abundant internal modification, which contributes to various steps of RNA metabolism (27, 28). Recently, RNA m6A modification has been reported to be involved in recruiting Y-family DNA repair DNA Pol κ to facilitate DNA repair and promote cell survival during ultraviolet irradiation (UV)-induced DNA damage response (DDR) (29). Notably, we have previously demonstrated that DNA Pol η and Pol κ are essential for HBoV1 DNA replication in both dividing HEK293 cells and the nondividing cells of HAE (30, 31).

In this study, we aimed to elucidate the mechanism underlying the requirement of BocaSR in HBoV1 DNA replication. We first determined and validated the in vivo secondary structure of BocaSR in HBoV1-infected HAE using dimethyl sulfate (DMS)-mutational profiling with sequencing (MaPseq). Our findings revealed that BocaSR is m6A-modified at multiple sites, which colocalizes with DNA Pol η and Pol κ. Most importantly, we uncovered that BocaSR interacts with a region of DNA spanning the viral DNA replication origin (*Ori*) at the REH in vitro. This interaction likely allows the m6A-modified BocaSR to act as a signal to recruit DNA Pol η and Pol κ to the viral *Ori*, thereby enhancing the DNA replication of HBoV1 in host cells.

Results

Determination of the In Vivo Structure of BocaSR in HBoV1-Infected Cells. To understand the role of BocaSR in HBoV1 DNA replication, we aimed to reveal the secondary structure of BocaSR, in vivo, during infection. To this end, we used DMS-MaPseq to probe the in vivo secondary structures of BocaSR in HBoV1-infected HAE cultured at an air–liquid interface (HAE-ALI) (32–34) (Fig. 1 *A*–*D*). DMS is a cell-permeable methylation reagent that reacts with RNA nucleobases and provides base pair information on the

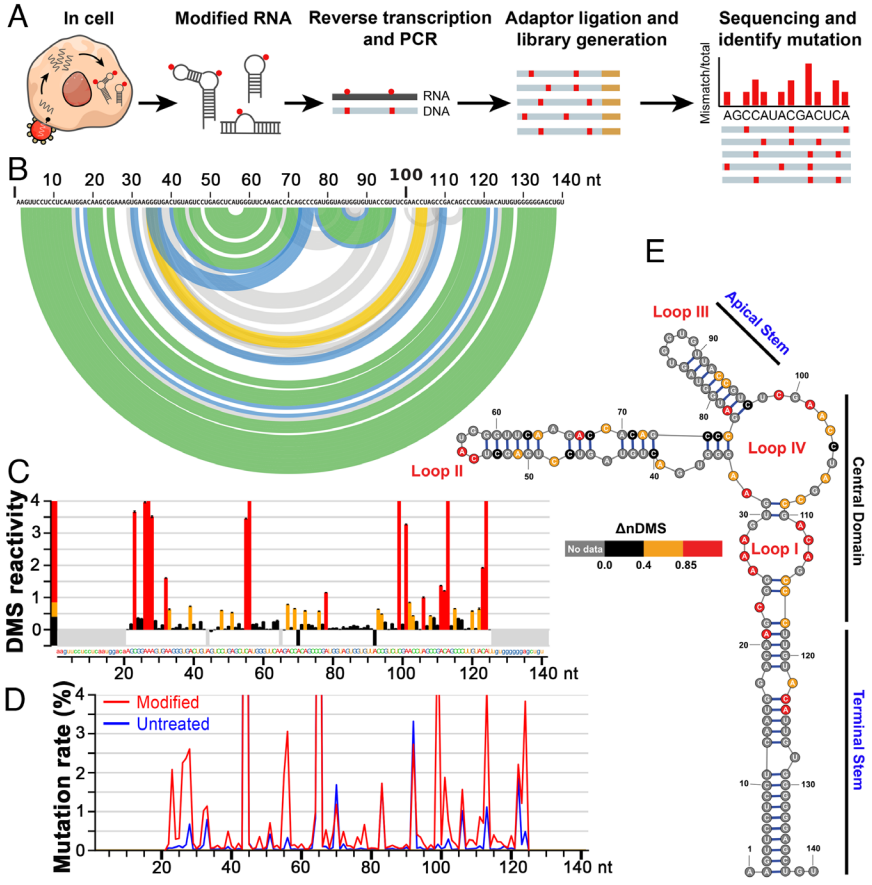

Fig. 1. Determination of the secondary structures of BocaSR in HBoV1-infected primary HAE-ALI. DMS was complemented in the medium of HBoV1-infected HAE-ALI cells before the extraction of total RNA and DMS-MaPseq. (*A*) Experiment procedures. The pipeline of in vivo DMS-MaPseq is outlined. (*B*) Arc plot of the most probable base-pairing pattern in BocaSR based on in-cell DMS-MaPseq data. The base pair probability is represented in green (80 to 100%), blue (30 to 80%), yellow (10 to 30%), or gray (<10%). (*C*) Histogram profile depicting DMS reactivity of BocaSR in HBoV1-infected primary HAE-ALI cells. The nucleotides and numbering across the *x* axis represent the sequence of BocaSR. Highly reactive nucleotides are depicted in red, medium in orange, and low in black. Regions that do not contain structural information are colored in gray. Error bars indicate SD from duplicate experiments. (*D*) Detection of the mutation rate in BocaSR. Mutation rates for BocaSR extracted from DMS-treated and untreated cells are plotted to the BocaSR sequence. (*E*) Determined in vivo BocaSR structure. The BocaSR secondary structure was generated by the ShapeMapper2 (35). A high normalized DMS activities (ΔnDMS) score indicates high DMS accessibility and low base pair probability. No data were used for G, U, and primer binding regions. Nucleotides of the BocaSR sequence are shown. Determined stems, central domain, and loops structures are indicated.

nucleotides adenine (A) and cytosine (C). Because unpaired ssRNA regions are more accessible to DMS modifications, DMS reactivities can be used to deconvolute RNA secondary and tertiary structures (33). Briefly, we treated HBoV1-infected HAE-ALI with DMS, extracted the total RNA, and used an established sequencing-based mutational profiling (MaP) approach to quantify DMS reactivities at a single nucleotide resolution (34). We specifically used an integrated analytical pipeline, ShapeMapper2 (35), for MaP and to assemble the most probable RNA structures by matching DMS activities and Shannon entropy analysis using SuperFold (36). A single stable BocaSR conformation was observed with stem-loop structures in infected HAE-ALI (Fig. 1*E*). Antisense oligonucleotides (ASOs) are able to change the functions and structures of the target RNA or mask the recruitment of RNA-binding proteins by forming Watson base pairs (37). To validate the function of the MaPseq determined in vivo structure, stems and loops, of BocaSR, ASOs targeting the stems and loops (*SI Appendix*, Fig. S1*A*) were applied to HEK293 cells before transfection of pIHBoV1, an infectious clone of HBoV1. pIHBoV1 replicates in HEK293 cells and produces progeny virions that are infectious to HAE-ALI (5). At 48 h posttransfection (hpt), replication of HBoV1 DNA was analyzed by Southern blotting, and the data showed that the ASOs targeting the loops I and IV (*SI Appendix*, Fig. S1*A*, ASO-1 and ASO-2) significantly inhibited viral DNA replication in a dose-dependent manner (*SI Appendix*, Fig. S1*B*, lanes 4 to 8 and 9 to 13, and *SI Appendix*, Fig. S1*C*). The replication of HBoV1 DNA was completely abolished with the addition of ASO-1 at 100 μM and ASO-2 at 10 μM, indicating the essential role of loops I and IV in virus replication. However, the control ASOs (ASO^{Ctrl1}, ASO^{Ctrl2}, and ASO^{Ctrl3}) targeting the stems (*SI Appendix*, Fig. S1*A*) did not inhibit HBoV1 DNA replication even at 100 μM (*SI Appendix*, Fig. S2 *A* and *B*, lanes 5, 7, and 9).

Taken together, we determined the in vivo structure of BocaSR and demonstrated the differential functions of the stem and loop structures of BocaSR in viral genome replication.

The Primary Modification of BocaSR Is m6A-modified. Transcribed by an intragenic RNA Pol III promoter, BocaSR shares similarities with transfer (t)RNAs in secondary structure (10, 38), yet its nuclear localization and the role in viral replication resemble those of EBERs. While tRNAs contain the largest numbers of modifications (39), EBER1 was found to carry a m5C modification (26). Thus, we screened RNA modifications (m6A, m5C, m7G, o8G, and Ψ) in BocaSR extracted from pIHBoV1-transfected HEK293 cells and HBoV1-infected HAE-ALI by using methylated RNA immunoprecipitation (MeRIP)-qPCR. The data revealed that BocaSR was highly m6A-modified in HEK293 cells (Fig. 2*A*, m6A = 99.998%, vs other modifications in Fig. 2 *B*–*E*, m5C = 1.427%, m7G = 10.136%, o8G = 0.259%, and Ψ = 9.107%), as well as in HBoV1-infected HAE-ALI (Fig. 2*F*, m6A = 99.782%).

To further validate the m6A modification of BocaSR, we used a PLA, in which BocaSR was recognized by four biotin-labeled oligo probes in an RNA fluorescence in situ hybridization (FISH), and the m6A modification was detected with an anti-m6A antibody. The specificity of the BocaSR FISH has been confirmed previously (10). Positively amplified fluorescent signals (Fig. 2 *G* and *H*, green) were detected in both pIHBoV1-transfected HEK293 cells and HBoV1-infected HAE-ALI, but not in mock-infected HAE-ALI cultures, indicating the colocalization of m6A and BocaSR. The vanishment of the amplified signals in both transfected/infected cells treated with RNase A (Fig. 2 *G* and *H*, RNase A+) further confirmed the m6A modification in BocaSR.

Taken all these data together, we evidenced that HBoV1 BocaSR was m6A-modified in both HBoV1 DNA replication and infection systems.

Silencing of m6A Processing Genes Inhibits HBoV1 DNA Replication. Because methyltransferases deposit m6A to RNAs in the nucleus (40), we first examined the role of m6A "Writer" methyltransferases, METTL3 (methyltransferase 3), METTL4, METTL14, and METTL16 (41), in HBoV1 DNA replication. We used Writer-specific shRNA-expressing lentiviral vectors to respectively silence each of the Writer genes in HEK293 cells (Fig. 3*A*), followed by transfection of pIHBoV1. At 2 d posttransfection (dpt), the cells were lysed, and the lower molecular weight (Hirt) DNA was extracted for Southern blotting (Fig. 3*B*). Quantification of the monomeric replicated form (mRF) DNA showed that viral DNA replication was inhibited by ~80% in the four m6A Writer-silenced cell lines (Fig. 3*B*, lanes 4 to 7 and Fig. 3*C*), compared with that in the scramble shRNA (shScram)-expressing cells (Fig. 3*B*, lane 3). As controls, in the four m6A Writer-silenced cell lines, BocaSR was m6A-modified at significantly lower levels, compared with that in the Scram control cells (*SI Appendix*, Fig. S3). Next, we silenced the genes encoded m6A "Reader," YT521-B homology (YTH) domain family of proteins (42), YTHDF1, YTHDC1, YTHDF2, and YTHDF3 (*SI Appendix*, Fig. S4*A*), and observed decreased viral DNA replication by 80 to 95% in each gene-silenced cell line (*SI Appendix*, Fig. S4 *B* and *C*).

Collectively, these results confirmed that m6A modification had a critical effect on HBoV1 DNA replication. Silencing of the *METTL3* (Writer) and the *YTHDC1* (Reader) led to substantial reductions of ~80% and ~95%, respectively, in HBoV1 DNA replication, representing the most significant effects among the tested Writer and Reader genes.

BocaSR m6A Modification Is Critical for HBoV1 DNA Replication. Now that we confirmed BocaSR is highly m6A methylated and m6A modification plays an important role in HBoV1 DNA replication, we further mutated the potentially modified adenosine (A) sites of BocaSR to determine whether such mutations functionally impact viral DNA replication. To maintain and ensure the secondary structure is unchanged, we mutated the predicted modified A sites to guanine (G) in BocaSR (*SI Appendix*, Fig. S5) (43). These sites are consistent with the m6A-conserved purine (G>A) m6AC(A/C/U) motif (44) or the sequence-based RNA Adenosine Methylation site Predictor (SRAMP) (45). The M-fold (46) and Kinefold (47) predictions showed these mutations retain the secondary structure of BocaSR (*SI Appendix*, Fig. S5, *D*–*H* vs. *A*). Two BocaSR mutants that had random mutations on A, which are not predicted to be m6A-modified, were used as controls (*SI Appendix*, Fig. S5 *B* and *C*). These BocaSR-mutated pIHBoV1 mutants were transfected into HEK293 cells to test their DNA replication. The data showed that the efficiency of HBoV1 DNA replication was significantly decreased in the cells expressing the m6A-depleted BocaSR (Fig. 4*A*, lanes 5 to 9 vs. 2), which had the lowest level (5%) of viral DNA replication in the combined m6A-depleted BocaSR-expressing cells (Fig. 4*A*, lane 8 and Fig. 4*B*, M4). For controls, the mutants with random mutations showed no significant difference in HBoV1 DNA replication (*SI Appendix*, Fig. S6).

As the function of m6A is mediated by m6A processing proteins (48), we then investigated whether these proteins directly bound to BocaSR. To this end, we conducted RNA pulldown experiments with the lysates of p3Z-BocaSR-, p3Z-$BocaSR^{Ctrl1}$-, and p3Z-$BocaSR^{M4}$-transfected HEK293 cells using an anti-m6A antibody. The data showed that m6A Writers, METTL3 and METTL14, "Eraser" FTO (alpha-ketoglutarate dependent dioxygenase FTO), and Reader YTHDC1 were pulled down in the lysates of BocaSR- and $BocaSR^{Ctrl1}$-expressing cells (*SI Appendix*, Fig. S7, lanes 3 and 4), but not in the lysate of $BocaSR^{M4}$-expressing cells (*SI Appendix*,

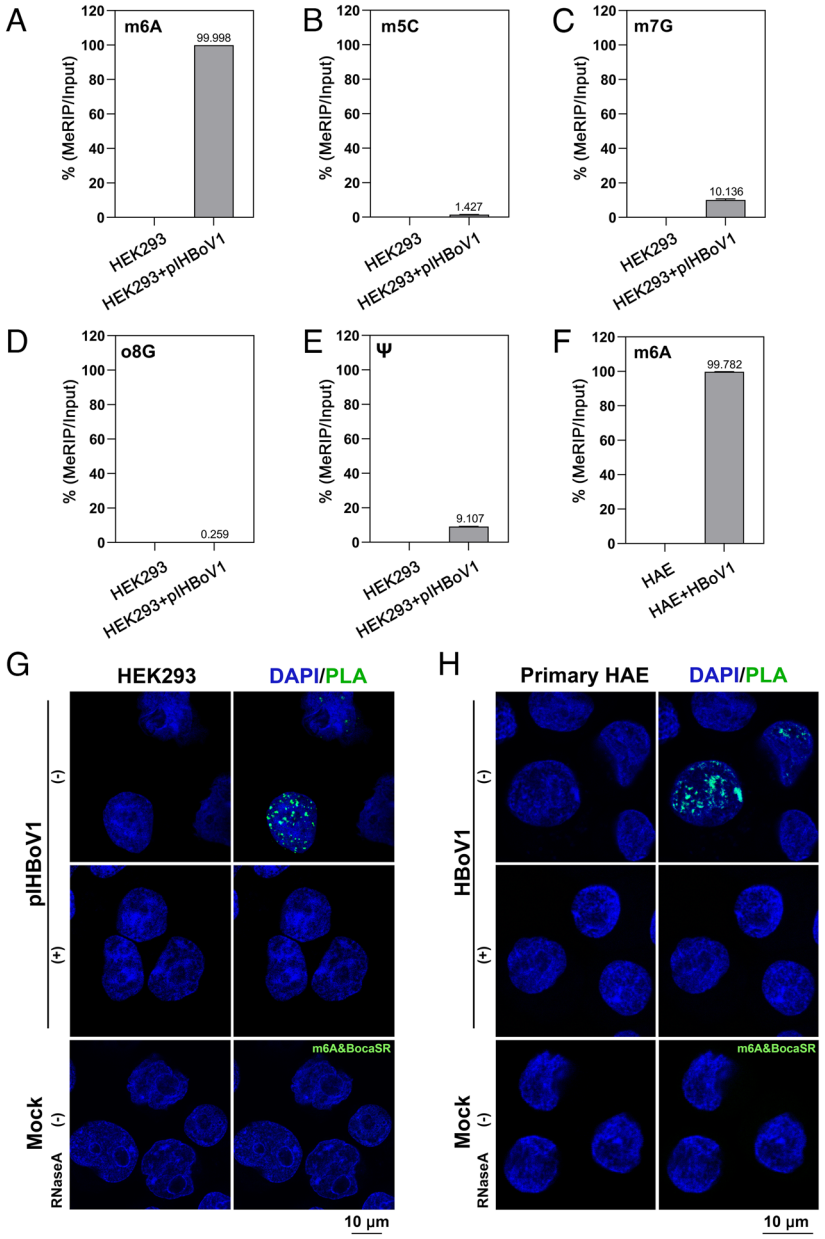

Fig. 2. BocaSR carries N6-methylated adenosines. (*A*–*F*) Methylated RNA immunoprecipitation–qPCR (MeRIP-qPCR). Total RNA of pIHBoV1 transfected HEK293 cells was prepared at 3 dpt (*A*–*E*). Total RNA of mock- and HBoV1-infected HAE ALI was prepared at 28 dpi (*F*). The RNA modifications existed in BocaSR were screened by using a BocaSR-specific MeRIP-qPCR, including N6-methyladenosine (m6A, *A* and *F*), 5-methylcytosine (m5C, *B*), N7-methylguanosine (m7G, *C*), 8-oxoguanine (o8G, *D*), and pseudouridine (Ψ, *E*). Data shown are percentages of MeRIP/input in pIHBoV1-transfected HEK293 cells vs mock-transfected cells (*A*–*E*) or HBoV1-infected HAE-ALI vs. mock-infected cultures (*F*), and were obtained from three different repeats. (*G* and *H*) Proximity ligation assay (PLA). HEK293 cells transfected with pIHBoV1 or mock-transfected were cytospun onto slide at 3 dpt (*G*). Cells of the HAE-ALI cultures infected with HBoV1 or mock-infected were cytospun onto slide at 16 dpi (*H*). After fixation and permeabilization, BocaSR was detected by biotin-labeled probes, followed by costaining with a rabbit anti-m6A and a mouse anti-biotin antibody for PLA. The amplified signals were visualized under a Leica TCS SP8 STED 3× super-resolution microscope. Nuclei were stained with DAPI. RNase A-treated transfected or infected cells were used as control. (Scale bar, 10 μm.)

Fig. S7, lane 5), confirming the interaction between BocaSR and the m6A processing proteins. The levels of BocaSR were confirmed by a BocaSR-specific reverse transcription-quantitative (RT-q) PCR assay. There were no significant differences in the total expression levels of BocaSR and its mutants in the cell lysates before the pulldown (*SI Appendix*, Fig. S7*B*), but a significant decrease in the pulldown BocaSR^{M4} from the lysate of BocaSR^{M4}-expressing cells, compared with that from the lysates of BocaSR- or BocaSR^{Ctrl1}-expressing cells (*SI Appendix*, Fig. S7*C*). To confirm the interaction of BocaSR with the m6A Writer, Eraser, and Reader, we carried out reverse pulldown assays using anti-METTL3, anti-FTO, and anti-YTHDC1 antibodies, respectively. The results showed that while BocaSR was efficiently pulled down, significantly less BocaSR^{M4} (>10-fold) was captured by these antibodies (*SI Appendix*, Fig. S8).

These results combined demonstrated that BocaSR was methylated at N6 of eight A sites (nt18, 39, 67, 70, 92, 102, 111, and 122) and that m6A Writers (METTL3, METTL14, and METTL16), Eraser (FTO), and Reader (YTHDC1) were complexed with BocaSR.

BocaSR m6A-Depleted HBoV1 Mutants Are Replication-Defective in the Human Airway Epithelium. Next, we examined the replication of BocaSR m6A-depleted HBoV1 (virus) mutants in polarized HAE-ALI cultures, which is an in vitro virus infection model mimicking virus infection of human

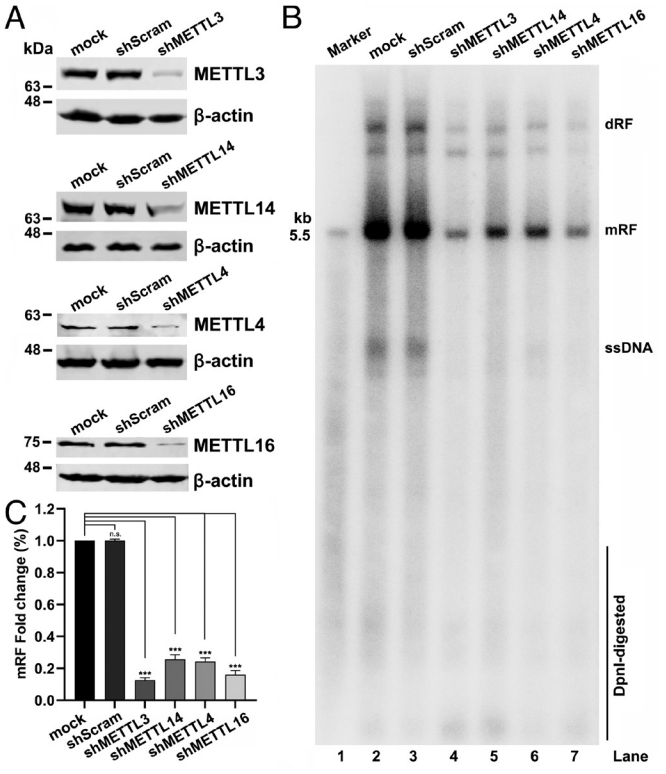

Fig. 3. Silencing of endogenous m6A Writer genes diminishes HBoV1 DNA replication. (*A*) Western blotting. In HEK293 cells, the m6A Writer genes, *METTL3*, *METTL14*, *METTL4*, and *METTL16*, were knocked down, using shRNA-expressing lentiviral vectors. shScram was used as a control. After the establishment of the cell lines, the cells were harvested for western blotting of Writer gene expression. β-actin was probed as a loading control. (*B*) Southern blotting. The established cell lines were transfected with pIHBoV1. At 2 dpt, cells were harvested for Hirt DNA preparation. The Hirt DNA was digested with DpnI and resolved in 0.9% agarose gel for Southern blotting, which used a full-length HBoV1 genome as the probe. DpnI-digested band was probed as a loading control. dRF, mRF, and ssDNA represent dimer, monomer replicative form DNA, and single-stranded DNA, respectively. HBoV1 duplex DNA excised from pIHBoV1 was used as a size marker (lane 1, marker, ~5.5 kb). (*C*) Quantification of mRF DNA. The intensity of mRF DNA bands was quantified using ImageQuant Tl software. The shown values are the relative fold reduction of the mRF (mean ± SD, obtained from three blots), normalized to the replication of pIHBoV1 in mock-transduced cells, which is arbitrarily set to 1. The shown data were analyzed by Student's *t* test (n.s., not significant; ***$P < 0.001$).

airways (1, 2, 5, 49). The pIHBoV1 derivatives containing various m6A-depletions in BocaSR were transfected into HEK293 cells to generate m6A-depleted HBoV1 mutants. As expected, the mutant titers were decreased (Fig. 5*A*), especially in HBoV1^{m6A}M4, which was consistent with the results from the pIHBoV1^{m6A}M4-transfected HEK293 cells (Fig. 4*A*, lane 8). The mutants were used to infect HAE-ALI at a multiplicity of infection (MOI) of 100 DNase I digestion-resistant particles (DRP)/cell, along with the wild-type (WT) HBoV1 as control. During a period of 16 d postinfection (dpi), apical washes were collected for quantification of progeny virions released using qPCR at an interval of 2 d. Starting from 6 dpi, the levels of the apical virus released from the infections of HBoV1 mutants (M1 to M5) were significantly lower than those from WT HBoV1 (Fig. 5*B*, M1 to M5 vs. HBoV1 and Ctrls). The mutant HBoV1^{m6A}M4 demonstrated the lowest replication efficiency with a titer ~6-log lower than WT. Because HBoV1 infection in HAE-ALI induces epithelial barrier dysfunction (5, 31), we determined the barrier function of the infected HAE by assessing the transepithelial electrical resistance (TEER) of the ALI cultures. The data showed that the TEER of the HBoV1^{m6A}M4-infected HAE-ALI was similar to the mock-infected control (Fig. 5*C*), and no significant dissociation of the tight junction (ZO-1 staining) or loss of cilia (β-tubulin IV staining) was found in HBoV1^{m6A}M4-infected HAE-ALI (Fig. 5 *D* and *E*, M4 vs. Mock). The controls HBoV1^{m6A}Ctrl1 and HBoV1^{m6A}Ctrl2 did not behave any different regarding virus titer, apical virus release, TEER, and staining of ZO-1 or β-tubulin IV, compared with the WT HBoV1 (Fig. 5, Ctrl1 and 2 vs. WT).

Collectively, these results demonstrated that depletion of m6A modification of BocaSR significantly reduced the infectivity and replication efficiency of the virus, as well as the airway epithelial barrier dysfunction caused during virus infection.

METTL3 Colocalizes with BocaSR and Facilitates HBoV1 Replication in the HBoV1-Infected Human Airway Epithelium. We further confirmed the colocalization of BocaSR and METTL3, the major BocaSR Writer in the m6A methyltransferase complex, in HBoV1-infected HAE-ALI using RNA fluorescence in situ hybridization (FISH) assay (Fig. 6*A*). This colocalization was also confirmed by proximity ligation assay (PLA) (Fig. 6*B*), as evidenced by the amplified fluorescent signals in HBoV1-infected cells but not in mock-infected cells. Next, we validated the functional involvement of the METTL3 in HBoV1 replication in HAE-ALI. We used an immortalized human airway epithelial cell line, CuFi-8 (50), to establish a single cell-derived *METTL3* knockout (KO) cell line (CuFi^{METTL3KO}) and generated a lentivirus expressing a codon-optimized *(opt)METTL3* for functional complementation of *METTL3* in the CuFi^{METTL3KO} cell line. After western blotting confirmed the *METTL3* KO and complementation of METTL3 from lentiviral vector transduction (Fig. 6*C*, lanes 3 and 5 vs. 2), we differentiated the CuFi^{METTL3KO} cells and the control counterpart cell line CuFi^{SsgRNA} at an ALI. These ALI cultures were infected with WT HBoV1, followed by determination of apical virus releases and TEER every 2 d. At 16 dpi, HAE-ALI^{METTL3KO} released virions at ~3 log less than that from the apical side, compared to the control (HAE-ALI^{SsgRNA}) (Fig. 6*D*). HAE-ALI^{METTL3KO} exhibited reduced infection-dependent barrier dysfunction (Fig. 6*E*). Importantly, the complementation of *optMETTL3* restored the apical virus release (Fig. 6*D*, HAE-ALI$^{METTL3KO+optMETTL3}$) and the airway epithelial damage, as determined by the disruption of TEER in METTL3-complemented HAE-ALI (Fig. 6*E*, HAE-ALI$^{METTL3KO+optMETTL3}$).

Collectively, these data confirmed the importance of m6A Writer METTL3 in HBoV1 replication of infected HAE-ALI.

m6A Modification Confers BocaSR to Recruit Y-Family DNA Polymerases. It was previously reported that m6A–RNA–METTL3 complex recruits DNA Pol κ to repair UV-damaged DNA (29). In our previous work, we demonstrated that HBoV1 utilizes Y-family DNA repair DNA Pol η and Pol κ for viral DNA replication (30, 31) and BocaSR localizes to the HBoV1 DNA replication centers (10). We hypothesized that the m6A methylation of BocaSR plays a crucial role in the recruitment of DNA Pol η and Pol κ to the HBoV1 DNA replication centers.

We next examined the colocalization of BocaSR with Pol η and Pol κ. As detected by FISH, BocaSR colocalized with both Pol η and Pol κ in the cells of HBoV1-infected HAE-ALI but not in HBoV1^{m6AM4} or mock-infected cells (Fig. 7 *A* and *B*). Moreover, in the experiments conducted in HEK293 cells transfected with p3Z-BocaSR or p3Z-BosaSR^{M4}, the colocalization of BocaSR with both Pol η and Pol κ was only detected in WT BocaSR-expressing cells, but not in mutant BocaSR^{M4}-expressing cells (Fig. 7 *C* and *D*). The colocalization of BocaSR with Pol η and Pol κ was further confirmed by a PLA assay in HBoV1-infected HAE-ALI (Fig. 7 *E* and *F*).

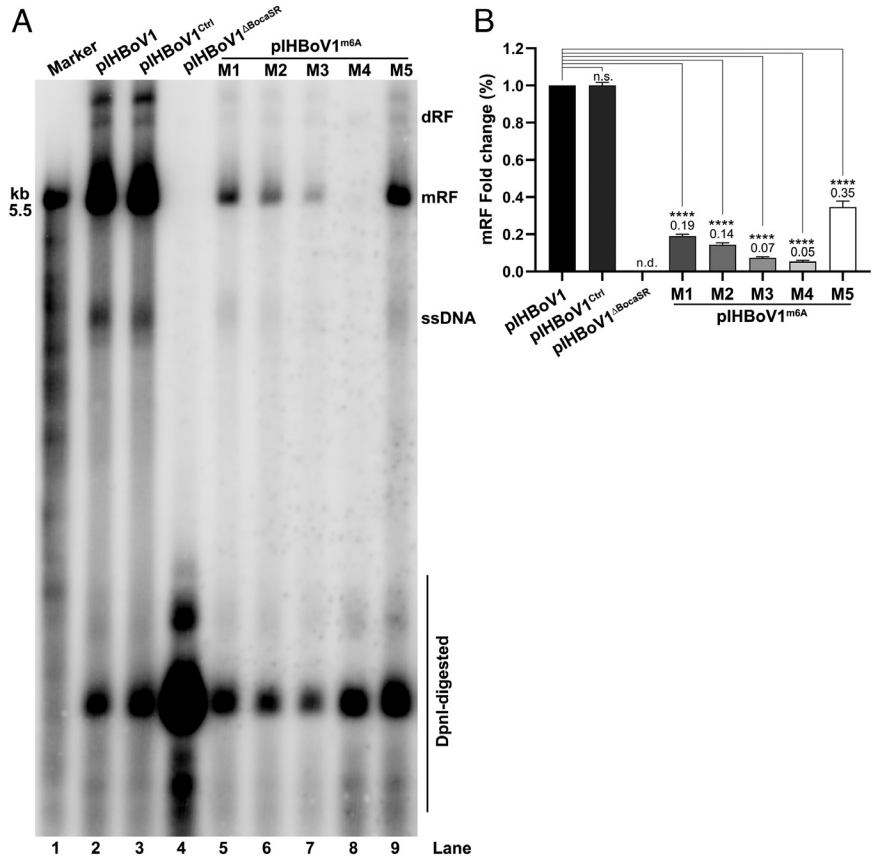

Fig. 4. Depletion of m6A modification of BocaSR diminishes HBoV1 DNA replication significantly. The potential m6A modification sites of the *BocaSR* gene in pIHBoV1 were mutated (*A* to *G*). Mutants: pIHBoV1^{m6A}M1(site: 18, in BocaSR), pIHBoV1^{m6A}M2 (sites: 18, 67, and 102), pIHBoV1^{m6A}M3 (sites: 18, 39, 67, 70, 102, 111, and 122), pIHBoV1^{m6A}M4 (sites: 18, 39, 67, 70, 92, 102, 111, and 122), and pIHBoV1^{m6A}M5 (site: 92). pIHBoV1^{Ctrl} and pIHBoV1$^{\Delta BocaSR}$ served as positive and negative controls, respectively. The indicated plasmids were transfected to HEK293 cells. (*A*) Southern blotting. At 2 dpt, Hirt DNA of the transfected cells was extracted, DpnI-digested, and subjected to Southern blotting. (*B*) Quantification of mRF DNA. The intensity of mRF bands was quantified by ImageQuant TL. The shown values are the relative fold reduction of the mRF (mean ± SD, obtained from three blots), normalized to the replication of pIHBoV1, which is arbitrarily set to 1. All the experiments were performed in triplicate, and the statistical analysis was carried out using Student's *t* test (n.s., not significant; n.d., not detectable; ****$P < 0.0001$).

These data generated from our colocalization experiments proved our hypothesis that the m6A methylation of BocaSR likely recruits the Pol η and Pol κ to the viral DNA replication centers where BocaSR localizes (10).

BocaSR Interacts with the REH of the HBoV1 Genome. As a base-pairing between EBER2 and nascent transcripts from the TRs of the EBV genome recruits the EBER2–PAX5 complex during viral lytic replication (17), we aligned the BocaSR sequence to the positive strands of HBoV1 LEH and REH, respectively, by using ClustalW (51). The alignments showed that BocaSR shares 42.67% identity in sequence with the LEH and 33.66% with the REH. To test a direct interaction between BocaSR and HBoV1 LEH or REH, we performed biolayer interferometry (BLI) assays. In this test, we synthesized oligonucleotides (oligos) based on the likely complementary regions between the LEH/REH and BocaSR (*SI Appendix*, Fig. S9), for an interaction with the biotin-dUTP labeled in vitro transcribed BocaSR or BocaSR^{M4}. The function of the in vitro transcribed BocaSR was validated with Southern blotting, which restored the loss of BocaSR in HBoV1 DNA replication (*SI Appendix*, Fig. S10, lanes 3 vs. 2). The data showed that BocaSR exhibited a binding parameter (an equilibrium dissociation constant [K_D]) of 1.2 nM with REH-1 oligo, and BocaSR^{M4} interacted with REH-1 at a K_D of 1.3 nM (*SI Appendix*, Fig. S11 *A*, *C*, and *E*). Both BocaSR and BocaSR^{M4} showed negligible binding kinetics with other oligos (motifs) derived from the LEH or REH (*SI Appendix*, Fig. S11 *B* and *D*). Notably, the REH-1 oligo largely covers the minimal viral *Ori* at the REH (*SI Appendix*, Fig. S9*B*) (6). As the data showed REH-1 potentially interacted with the region of nt 21 to 53 of BocaSR which spans loops I and IV (Fig. 1*E*), we tested oligos REH-1a and REH-1b for an interaction with BocaSR potentially at regions of nt 21 to 39 and nt 40 to 53, respectively (*SI Appendix*, Fig. S9*B*). The data showed that REH-1a oligo remained a high affinity binding with BocaSR at a K_D of 26.7 nM, but not the REH-1b oligo (Fig. 8 *A*–*C*).

Thus, the in vitro binding kinetics demonstrated a strong interaction between BocaSR and the *Ori* at the REH of HBoV1, indicating that BocaSR may bind to the unwound ssDNA at the *Ori* of the REH during HBoV1 DNA replication

Discussion

In this report, we revealed a mechanism underlying the requirement of a viral sncRNA in viral DNA replication. BocaSR is highly m6A-methylated and plays a crucial role in virus replication. Associated with the m6A processing complex, BocaSR interacts with the viral *Ori* and recruits the Y-family DNA repair DNA Pol η and Pol κ to the HBoV1 RIC (11) to facilitate viral DNA replication (Fig. 8*D*).

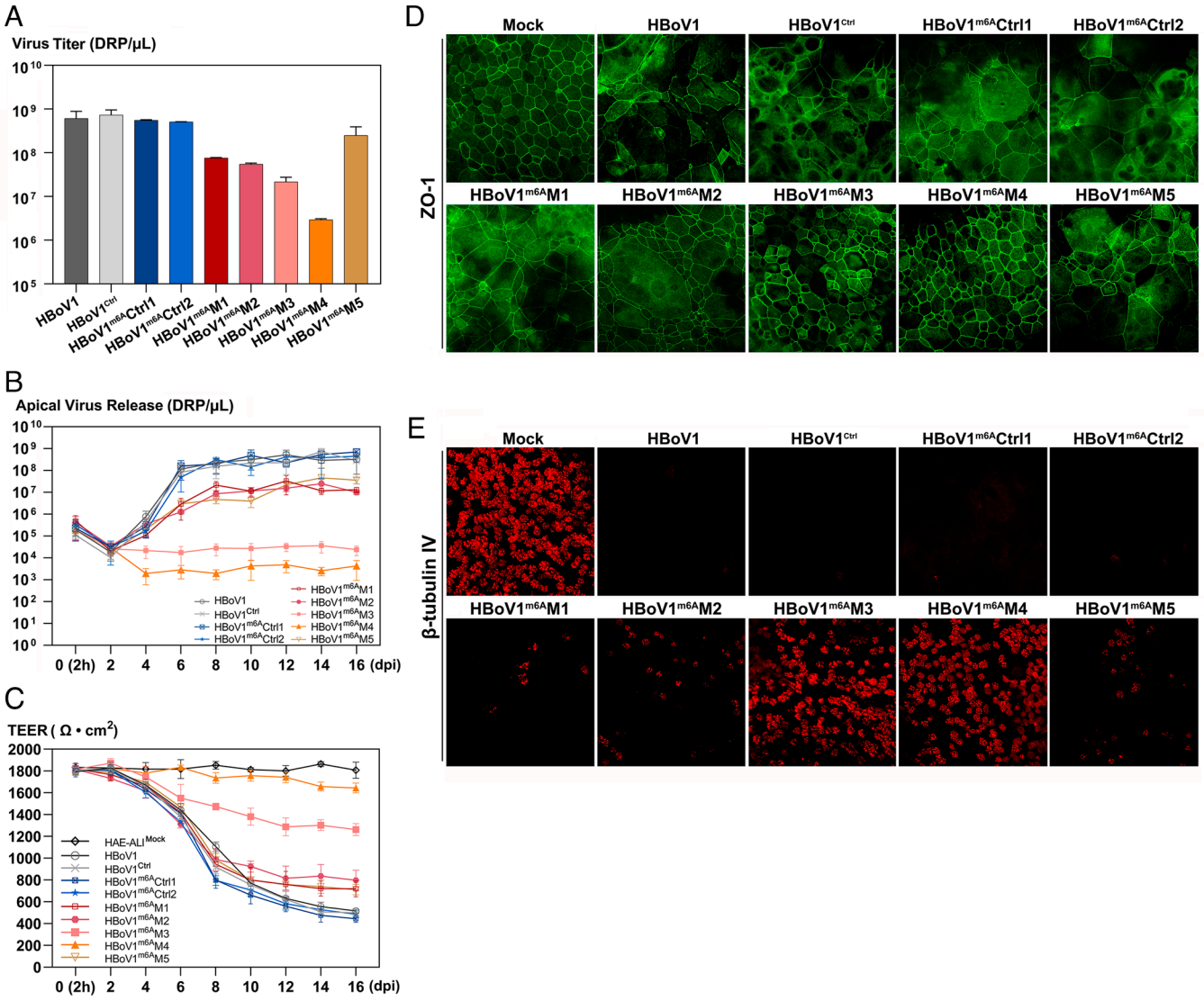

Fig. 5. BocaSR m6A modification decreases HBoV1 replication in HAE-ALI and abrogates the infection-caused epithelial barrier dysfunction. (*A*) Quantification of virus production. WT HBoV1, control (Ctrl; HBoV1^{Ctrl}, HBoV1^{m6A}Ctrl1, and HBoV1^{m6A}Ctrl2), and BocaSR m6A depleted-HBoV1 mutants (M1 to M5) were produced by transfection of HEK293 cells. At 72 hpt, the cells were harvested for virus preparation in 500 μL. The titers (DRP/μL) of the indicated viruses were detected by qPCR. Data shown are means ± SD from three different preparations. (*B–E*) Infection of HBoV1 in primary HAE-ALI. Primary HAE-ALI cultures were infected with WT HBoV1, and its mutants as indicated at an MOI of 100. (*B*) Apical virus release. Virus released in the apical chamber of the HAE-ALI cultures were collected over the course of 16 d. At the indicated dpi, the apical virus releases were collected in 100 μL of PBS and quantified by qPCR. Values shown represent means ± SD of the virus collected from three infected HAE-ALI cultures. (*C*) TEER measurement. At the indicated dpi, the TEER of mock and HBoV1-infected HAE-ALI cultures was measured and is shown in mean ± SD of three inserts. (*D* and *E*) Immunofluorescent analysis. At 16 dpi, the ALI membrane of the infected HAE-ALI was stained and visualized for ZO-1 (green, *D*) and β-tubulin IV (red, *E*) expression under a confocal microscope at a magnification of ×40. (Scale bar, 10 μm.)

BocaSR, a viral sncRNA, is essential for DNA replication of HBoV1 in both dividing HEK293 cells and nondividing cells of HAE-ALI (10). We previously determined the nucleotide sequence and predicted the structure of BocaSR in silico and showed there was a high similarity to Ad VA RNAI (~160 nt) (10, 52). Interestingly, mutations of single or dual nucleotides within BocaSR drastically decreased the ability of BocaSR in facilitating HBoV1 DNA replication (10), indicating the importance of determining the secondary structure of BocaSR in vivo. Herein, we determined and validated the in vivo secondary structure of BocaSR by using a chemical probing strategy, MaPseq (33), which we previously used to elucidate the structure of the 3′ UTR of SARS-CoV-2 genome in infected cells (34). The stem regions of BocaSR share a high similarity in sequence with VA RNAs (13). These sequences are highly conserved, particularly in the A-box and B-box, which serve as the key elements of the type II intragenic RNA Pol III promoter. Nevertheless, the previously predicated loops still fall largely in the current verified loops. Mutations in the loop regions of the predicted structure diminish the effectiveness of BocaSR in viral DNA replication (10), suggesting the importance of the loops for the functions of BocaSR in virus replication.

m6A is the most abundant internal modification in RNA transcribed by RNA Pol I [ribosome (r)RNA], RNA Pol II (mRNA and ncRNA), and RNA Pol III [small nuclear (sn)RNA], contributing to the metabolism of RNA, including viral RNA and mRNA (24, 28, 53, 54). RNA Pol III–transcribed ncRNAs (28), U6 snRNA (55) and 7SK snRNA (27), are m6A-methylated by METTL16 and METTL3, respectively. Eight m6A-modified sites on 7SK snRNA have been revealed, which facilitates the sequestration of positive transcription elongation factor b (p-TEFb) complex for mRNA transcription elongation (27). To

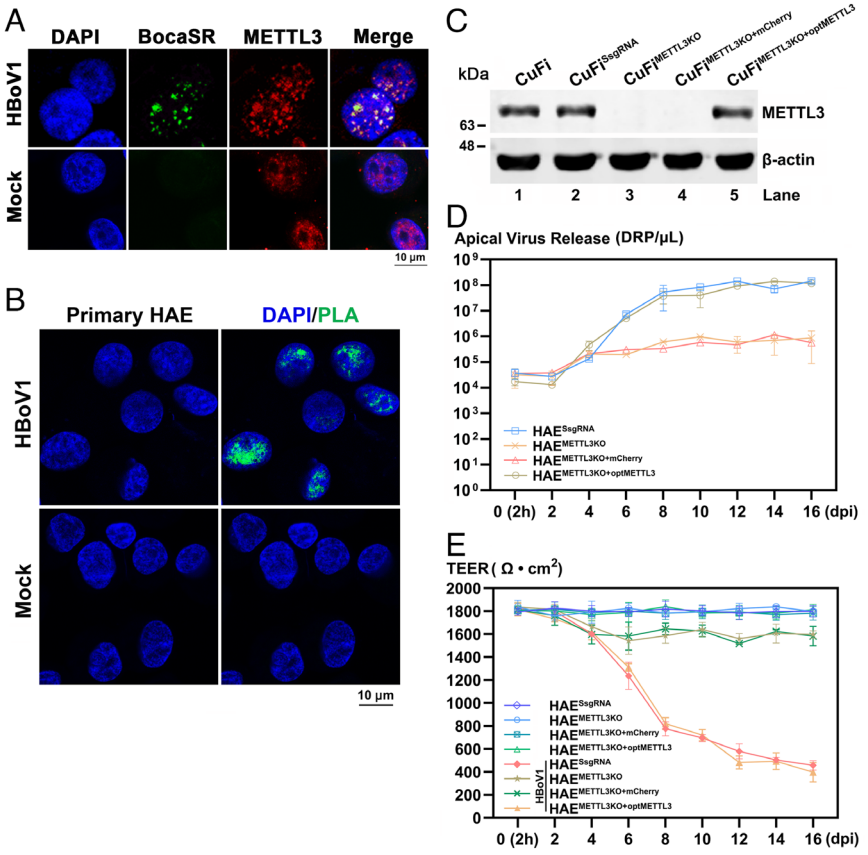

Fig. 6. METTL3 colocalizes with BocaSR and plays a crucial role in HBoV1 replication in HAE-ALI. (*A* and *B*) Colocalization of BocaSR and METTL3 in HBoV1-infected HAE-ALI. (*A*) Costaining of BocaSR and METTL3 for colocalization. Primary HAE-ALI cultures were infected with HBoV1 (MOI = 100 DRP/cell) or mock-infected. At 16 dpi, cells were digested off the insert of HAE-ALI and cytospun onto slide for staining of BocaSR by FISH (green) and METTL3 (red). (*B*) PLA for colocalization. The PLA was performed using a rabbit anti-METTL3 and a mouse anti-biotin antibody. The amplified signals (green) were visualized under a confocal microscope. The nucleus was stained by DAPI (blue). Mock-infected primary HAE-ALI served as a control. (Scale bar, 10 μm.) (*C*–*E*) HBoV1 infection in *METTL3* knockout (KO) HAE-ALI. (*C*) Western blotting. CuFi, CuFi^{SsgRNA} (served as control), CuFi^{METTL3KO}, CuFi$^{METTL3KO+mCherry}$ (served as a control), and CuFi$^{METTL3KO+optMETTL3}$ were detected for METTL3 expression using western blotting. β-actin serves as a loading control. (*D*) Apical virus release. HAE-ALI^{SsgRNA}, HAE-ALI^{METTL3KO}, HAE-ALI$^{METTL3KO+optMETTL3}$, and HAE-ALI$^{METTL3+mCherry}$ were infected with WT HBoV1 virus. Apical released virions were collected at 2-d intervals and quantified with qPCR. (*E*) TEER measurements. The TEER of the infected HAE-ALI cultures was measured over the course of infection. Data shown are means ± SD from three infected cultures.

date, limited modifications have been reported in viral ncRNAs. Although EBER1 is m5C-modified, no biological functional changes were observed during viral lytic replication (26). BocaSR and EBERs share similarities not only in sequence (~46%) but also in nuclear localization (10). They are both highly structured RNA Pol III–transcribed sncRNAs, and abundantly expressed in the nucleus of infected cells (10, 12). Instead of m5C, we found m6A methylation in eight positions of BocaSR. Interestingly, instead of the dependence on a specific m6A processing protein, knockdown of all the tested Writers and Readers of m6A resulted in various reduction of HBoV1 replication, indicating that there are redundant mechanisms underlying BocaSR m6A modification. This may also suggest that these m6A processing proteins have other functions, e.g., pre-mRNA processing, RNA stability of transcription, during HBoV1 replication. Nevertheless, mutating a single m6A-modified site resulted in a moderate decrease in viral DNA replication, however, the combined mutations of all eight m6A-modified sites nearly abolished viral DNA replication in both HEK293 cells (by transfection of an infectious clone) and HAE-ALI (by virus infection). Importantly, we determined the half-life of BocaSR (7.62 ± 0.32 h) and BocaSR^{M4} (7.67 ± 0.30 h) (*SI Appendix*, Fig. S12), confirming these combined mutations did not alter the stability of BocaSR. Thus, we have demonstrated the critical role of m6A modification of a viral RNA Pol III transcript in facilitation of viral DNA replication.

The molecular functions of METTL3-mediated m6A methylation are highly diverse, including but not limited to transcription regulation, splicing, polyadenylation, translation, and DNA repair (28, 48). It has been reported that m6A modification regulates the UV-induced DDR by recruiting DNA Pol κ to the DNA damage foci to facilitate DNA repair through interaction with the m6A–RNA–METTL3 complex (29). Notably, the HBoV1 genome possesses heterogeneous termini both at the 5' and 3' ends (LEH and REH), resembling a DNA molecule with characteristics similar to an ssDNA break that is recognized and repaired by the high-fidelity Y-family DNA polymerases Pol η and Pol κ through a DNA repair mechanism (30, 31). Our studies revealed the colocalization of METTL3, m6A-modified BocaSR, and Pol η or Pol κ, and more importantly, the complex of METTL3 and m6A-modified BocaSR and the colocalization of BocaSR with Pol η and Pol κ in cells of HBoV1-infected HAE-ALI and HEK293 cells expressing BocaSR only (Fig. 7 *C* and *D*). These lines of evidence suggest a possibility that the m6A-modified BocaSR is complexed with METTL3 and then actively recruits Pol η and Pol κ to the HBoV1 *Ori* (Fig. 8*D*), which is essential for HBoV1 DNA replication.

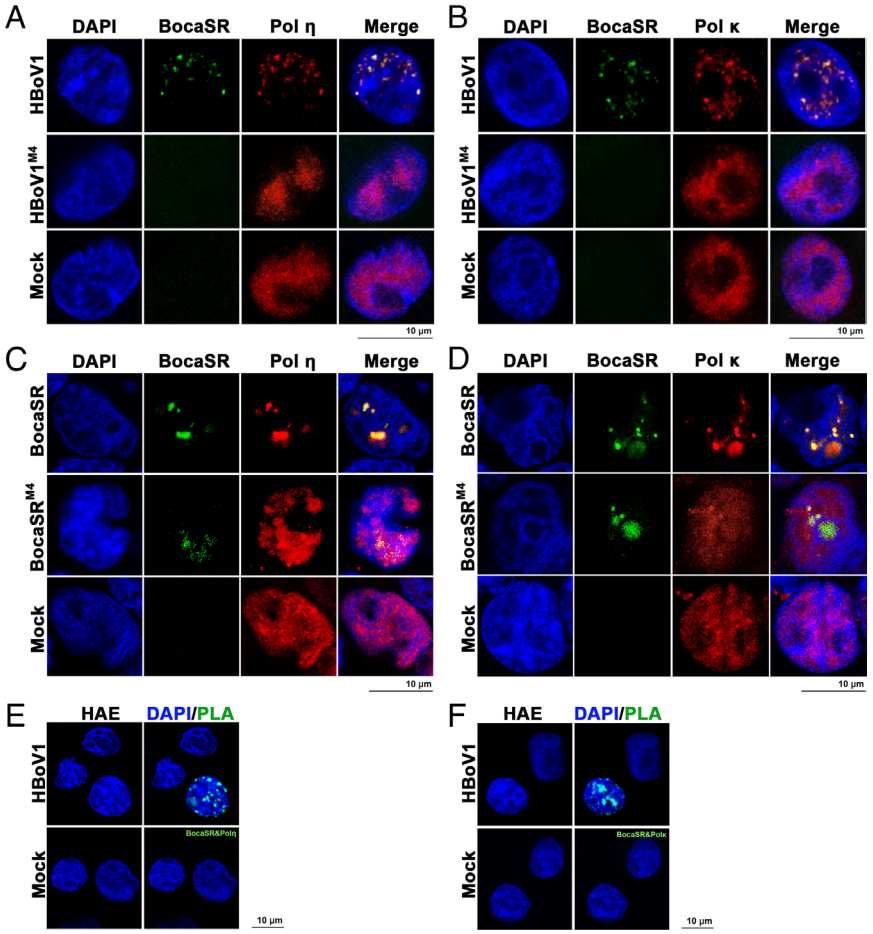

Fig. 7. m6A-modified BocaSR colocalizes with DNA Pol η and Pol κ in HBoV1-infected primary HAE-ALI as well as in BocaSR-only-transfected HEK293 cells. (*A*–*D*) Costaining of BocaSR/BocaSR^{m4} with Pol η and Pol κ. (*A* and *B*) WT HBoV1-/ HBoV1^{M4}-infected primary HAE-ALI cultures. Primary HAE-ALI was infected with WT HBoV1 or HBoV1^{M4} at an MOI of 100. At 16 dpi, the cells were detached from the inserts and cytospun onto slide for costaining of BocaSR and Pol η (*A*) or Pol κ (*B*). (*C* and *D*) BocaSR-/BocaSR^{M4}-expressing HEK293 cells. p3Z-BocaSR and p3Z-BocaSR^{M4} were transfected into HEK293 cells, respectively. At 3 dpt, the cells were collected and cytospun onto slides for costaining of BocaSR and Pol η (*C*) or Pol κ (*D*). BocaSR was detected by a FISH assay using biotin-labeled probes. Pol η (*A* and *C*) or Pol κ (*B* and *D*) was stained with a specific antibody, followed by staining with respective secondary antibodies. (*E* and *F*) PLA in HBoV1-infected primary HAE-ALI. The PLA was performed using rabbit anti-Pol η/Pol κ and a mouse anti-biotin antibody. The amplified signals were visualized under a confocal microscope. The nucleus was stained with DAPI. Mock primary HAE-ALI and HEK293 cells served as a negative control. (Scale bar, 10 μm.)

METTL3-mediated m6A methylation occurs on mRNA and other RNA Pol II transcripts that form R-loops, the structures composed of an RNA-DNA hybrid and a complementary ssDNA (28, 56). These R-loop structures are involved in DNA repair and transcriptional regulation (57). The high affinity interaction of the loop region (loops I and IV, Fig. 1*E*) of BocaSR with the viral DNA replication region of the HBoV1 REH (6), which is also in a form of RNA-DNA hybrid (Fig. 8*D*), highlights the importance of the accumulation of BocaSR to the viral *Ori* mediated by m6A methylation. During parvoviral DNA replication, the viral *Ori* is unwound by the large nonstructural protein NS1 and cellular helicases (58). This function presents the viral *Ori* as an ssDNA form and likely confers an RNA-DNA interaction between BocaSR and the viral ssDNA (Fig. 8*D*). However, EBER2 enhances EBV lytic replication through an RNA–RNA interaction. EBER2 binds to the nascent RNA transcripts from the TRs of the EBV genome, which brings the EBER2-bound PAX5 in proximity of the TRs (17). Apparently, viral sncRNA exhibits their functions through various interactions to DNA, RNA, or proteins. The ribonucleoprotein (RNP) of sncRNA, i.e., 7SK snRNP, is dynamic and that the RNA structure and protein interactions change in response to cellular conditions to control the activity (59, 60). It is likely that the secondary structure of viral sncRNA is dynamic in response to various interacting partners during virus replication, which warrants further investigation.

EBERs and VA RNAs interact with host proteins for their transport and processing, while also regulating the syntheses of both host and viral proteins (12). It has been reported that RNA modifications and structures cooperate to guide RNA–protein interactions (41). BocaSR, VA RNAs, EBERs, and cellular tRNA are all transcribed by an RNA Pol III promoter and shared similar secondary structures (10, 12). The diverse functions of BocaSR in viral protein expression suggest that in addition to its functional role in viral DNA replication that requires m6A modification, it may interact with host proteins, potentially by regulating viral RNA transcription and translation (10). Certainly, further investigation is needed to fully understand the distinct functions of BocaSR in HBoV1 replication.

In conclusion, we demonstrated the unique function of the m6A modification of BocaSR, an RNA Pol III–transcribed sncRNA, in parvoviral DNA replication. This process resembles DNA repair processing using the high-fidelity Y-family DNA Pol η and Pol κ. Thus, our niche viral DNA replication systems in both dividing (30) and nondividing (31) cells provide a simple model that can be used to study DNA repair and m6A modification.

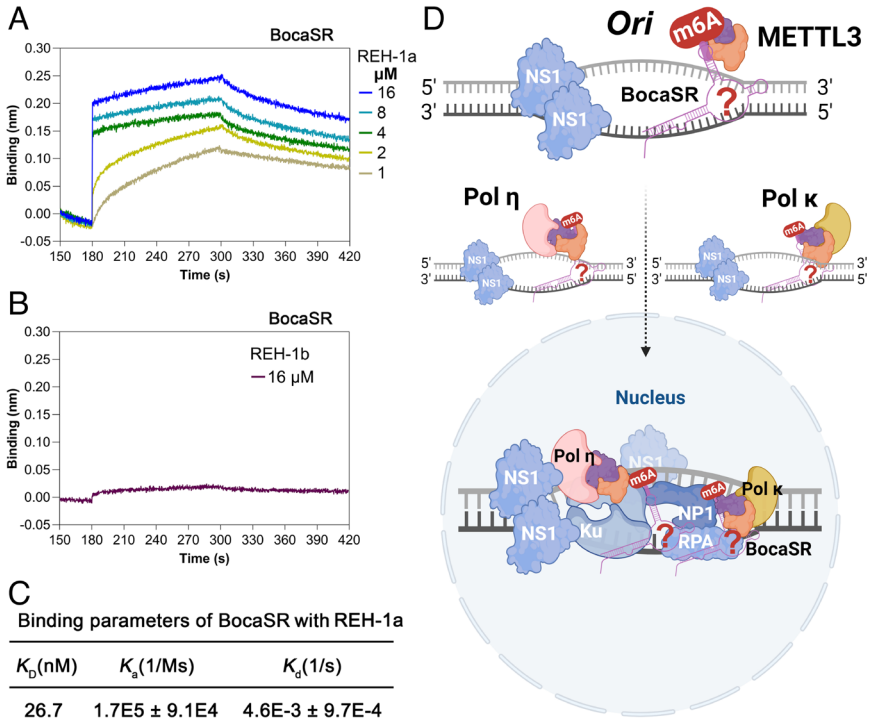

Fig. 8. BocaSR interacts with the unwound viral *Ori* of the REH, which likely recruits DNA Pol η and Pol κ to the HBoV1 replication initiation complex (RIC). (*A* and *B*) Kinetics of the in vitro interaction of oligos REH-1a/b with BocaSR. Oligos REH-1a and REH-1b are located within HBoV1 REH1 (*SI Appendix*, Fig. S9*B*), and their sequences are listed in *SI Appendix*, Table S3. Biotin-dUTP labeled BocaSR was mounted on streptavidin biosensors. The binding kinetics depicts the associations and dissociations of 80 pM BocaSR with oligoes REH-1a and REH-1b at indicated concentrations. (*C*) The binding parameters of BocaSR with REH-1a oligo. Equilibrium dissociation constant K_D value represents the ratio of dissociation [K_d (1/s)] and association [K_a (1/Ms)] computed from the real-time binding curves of BocaSR with REH-1a oligo. Data shown were generated from at least three repeated experiments. (*D*) A proposed model of BocaSR m6A-regulated HBoV1 DNA replication. The schematic model of the HBoV1 RIC was modified based on our previous publication (11). BocaSR is m6A-modified by the m6A-methyltransferase, which is complexed with the m6A processing proteins. BocaSR potentially interacts with the negative strand of the HBoV1 genome located in the *Ori* at the REH. The double-stranded DNA *Ori* is recognized by the viral large nonstructural protein NS1 and unwound through its helicase activity. Subsequentially, the BocaSR–m6A–METTL3 complex, which may be involved with other m6A processing proteins, then recruits Y-family DNA Pol η and Pol κ to the *Ori*, where cellular DNA damage/repair proteins, KU complex and replication protein A (RPA), and viral NP1 are localized, assembling RIC for viral DNA replication (11). Question markers indicate potential interactions among m6A modified BocaSR and HBoV1 *Ori*. The schematic model was created with BioRender.com.

Materials and Methods

Cell Lines and HAE-ALI Cultures. HEK293 cells (#CRL-1573, American Type Culture Collection [ATCC], Manassas, VA) and HEK293T cells (#CRL-11268, ATCC) were purchased from ATCC. Polarized primary HAE-ALI cultures were prepared by the Tissue and Cell Culture Core of the Center for Gene Therapy, University of Iowa. HAE-ALI cultures were also generated from the immortalized airway epithelial cell line CuFi-8 and *METTL3* gene knockout CuFi-8 cells. Details for all cell lines and cultures and differentiation procedures can be found in *SI Appendix*.

Plasmid Constructs, Transfection, Lentivirus Production, and Transduction. Information of plasmid construction and antisense oligonucleotides (ASO) and methods of plasmid and ASO transfections, lentivirus production, and transduction can be found in *SI Appendix*.

HBoV1 Production, Infection, and Quantification. pIHBoV1 or its mutants were transfected into HEK293 cells on 150-mm plates for virus production. Methods of virus production, infection, and quantification can be found in *SI Appendix*.

Determination of In Vivo Secondary Structures of BocaSR. HBoV1-infected HAE-ALI cells were used for in-cell DMS treatment. All samples were prepared in duplicates. Reverse transcription of DMS-treated and untreated RNA samples was conducted. Libraries were constructed and sequenced. Detailed methods can be found in *SI Appendix*.

Methylated RNA Immunoprecipitation (MeRIP) and MeRIP-qPCR. MeRIP was carried out using anti-m6A/m5C/m7G/o8G/Ψ antibodies, respectively. Immunoprecipitated BocaSR was quantified by RT-qPCR. Detailed methods can be found in *SI Appendix*.

Immunofluorescence Assay (IF), RNA FISH assay, and PLA. HEK293 cells or HAE cells disassociated from HAE-ALI cultures using Accutase were washed twice with PBS, cytospun onto slides, and fixed. IF, FISH, and PLA were carried out as described in *SI Appendix*. Nuclei were stained with DAPI. Confocal images were visualized under a Leica TCS SP8 STED 3× super-resolution microscope.

The RNA Immunoprecipitation (RIP) Assay. Cells were cross-linked in PBS with 1.0% formaldehyde for RIP assay. Details can be found in *SI Appendix*.

In Vitro Transcription of BocaSR and Transfection. BocaSR was in vitro transcribed by using an invitro RNA transcription Kit with complementation of Biotin-dUTP. The template was amplified by PCR detailed in *SI Appendix*. Lipofectamine 3000 (ThermoFisher) was used for transfection.

Biolayer Interferometry (BLI) Assay. A series of oligoes based on the sequences of HBoV1 LEH and REH were synthesized by IDT (*SI Appendix*, Table S3) and used for interaction with BocaSR in the BLI assay. The BLI kinetics analysis was performed on Octet Red96e (Sartorius, Bohemia, NY), with details provided in *SI Appendix*.

Western Blotting and Southern Blotting. Signals of western blots were visualized with an Odyssey imaging system (LI-COR, Lincoln, NE), and signals of Southern blots were visualized on the Amersham Typhoon Biomolecular Imager. Details were provided in *SI Appendix*.

Statistics Analysis. Statistical analysis was performed with GraphPad Prism (version 9.5, GraphPad software, Boston, MA). Data are representative of triplet experiments and shown as mean ± SD. Statistical significance *P* values were determined by using Student's *t* test. $^{****}P < 0.0001$, $^{***}P < 0.001$, $^{**}P < 0.01$, and $^{*}P < 0.05$ were regarded as statistically significant, and n.s. was regarded as statistically insignificant.

Data, Materials, and Software Availability. The FASTQ files for the DMS-MaPseq in this study are available from the National Center for Biotechnology Information Sequencing Read Archive (SRA) under BioProject accession # PRJNA955716 (61). All other data are included in the manuscript and/or *SI Appendix*.

ACKNOWLEDGMENTS. We thank the members of the Jianming Qiu Laboratory for their valuable discussions. We are indebted to Dr. Jianrong Li at the Ohio State University and Dr. Yan Xiang at University of Texas Health San Antonio for the kind of research materials and valuable discussions. We thank Dr. Yanggu Shi from Arraystar Inc. for technical support of MeRIP-qPCR. We thank Dr. Joe F. Lutkenhaus from the University of Kansas Medical Center for the support of the Biolayer Interferometry assay. We are also grateful for the support from Dr. John F. Engelhardt and the Center for Gene Therapy, the University of Iowa (National Institutes of Health (NIH) Grant P30DK054759). This study was supported by National Institute of Allergy and Infectious Diseases (NIAID) Grants AI150877 and AI156448 (Drs. Jianming Qiu and Ziying Yan), National Institute of General Medical Sciences (NIGMS) Grant R35 GM147498 (Dr. Jingxin Wang), and Cystic Fibrosis Foundation Research Grant YAN23G0 (Dr. Ziying Yan). We are grateful to the Confocal Microscopy Core Laboratory at The University of Kansas Medical Center. The Stimulated Emission Depletion (STED) confocal microscope was supported by NIH Grant S10 OD 023625. The funders had no role in the study design, data collection and interpretation, or the decision to submit the work for publication.

Author affiliations: [a]Department of Microbiology, Molecular Genetics and Immunology, University of Kansas Medical Center, Kansas City, KS 66160; [b]Department of Medicinal Chemistry, University of Kansas, Lawrence, KS 66045; [c]Section of Genetic Medicine, Department of Medicine, Biological Sciences Division, University of Chicago, Chicago, IL 60637; and [d]Department of Anatomy and Cell Biology, University of Iowa, Iowa City, IA 52242

1. A. Christensen *et al.*, Human bocaviruses and paediatric infections. *Lancet Child Adolesc. Health* **3**, 418–426 (2019).
2. J. Qiu, M. Söderlund-Venermo, N. S. Young, Human parvoviruses. *Clin. Microbiol. Rev.* **30**, 43–113 (2017).
3. T. Allander *et al.*, Human bocavirus and acute wheezing in children. *Clin. Infect. Dis.* **44**, 904–910 (2007).
4. S. F. Cotmore *et al.*, The family Parvoviridae. *Arch. Virol.* **159**, 1239–1247 (2014).
5. Q. Huang *et al.*, Establishment of a reverse genetics system for studying human bocavirus in human airway epithelia. *PLoS Pathog.* **8**, e1002899 (2012).
6. W. Shen *et al.*, Analysis of the cis and trans requirements for DNA replication at the right end hairpin of the human bocavirus 1 genome. *J. Virol.* **90**, 7761–7777 (2016).
7. A. Y. Chen *et al.*, Characterization of the gene expression profile of human bocavirus. *Virology* **403**, 145–154 (2010).
8. W. Shen *et al.*, Identification and functional analysis of novel non-structural proteins of human bocavirus 1. *J. Virol.* **89**, 10097–10109 (2015).
9. W. Zou *et al.*, Nonstructural protein NP1 of human bocavirus 1 plays a critical role in the expression of viral capsid proteins. *J. Virol.* **90**, 4658–4669 (2016).
10. Z. Wang *et al.*, Parvovirus expresses a small noncoding RNA that plays an essential role in virus replication. *J. Virol.* **91**, e02375-16 (2017).
11. K. Ning *et al.*, The small nonstructural protein NP1 of human bocavirus 1 directly interacts with Ku70 and RPA70 and facilitates viral DNA replication. *PLoS Pathog.* **18**, e1010578 (2022).
12. K. T. Tycowski *et al.*, Viral noncoding RNAs: More surprises. *Genes Dev.* **29**, 567–584 (2015).
13. Y. Ma, M. B. Mathews, Structure, function, and evolution of adenovirus-associated RNA: A phylogenetic approach. *J. Virol.* **70**, 5083–5099 (1996).
14. M. D. Rosa, E. Gottlieb, M. R. Lerner, J. A. Steitz, Striking similarities are exhibited by two small Epstein-Barr virus-encoded ribonucleic acids and the adenovirus-associated ribonucleic acids VAI and VAII. *Mol. Cell Biol.* **1**, 785–796 (1981).
15. T. Punga, M. Darweesh, G. Akusjärvi, Synthesis, structure, and function of human adenovirus small non-coding RNAs. *Viruses* **12**, 1182 (2020).
16. J. G. Howe, J. A. Steitz, Localization of Epstein-Barr virus-encoded small RNAs by in situ hybridization. *Proc. Natl. Acad. Sci. U.S.A.* **83**, 9006–9010 (1986).
17. N. Lee, W. N. Moss, T. A. Yario, J. A. Steitz, EBV noncoding RNA binds nascent RNA to drive host PAX5 to viral DNA. *Cell* **160**, 607–618 (2015).
18. I. A. Roundtree, M. E. Evans, T. Pan, C. He, Dynamic RNA modifications in gene expression regulation. *Cell* **169**, 1187–1200 (2017).
19. D. Dominissini *et al.*, Topology of the human and mouse m6A RNA methylomes revealed by m6A-seq. *Nature* **485**, 201–206 (2012).
20. J. E. Squires *et al.*, Widespread occurrence of 5-methylcytosine in human coding and non-coding RNA. *Nucleic Acids Res.* **40**, 5023–5033 (2012).
21. J. Létoquart *et al.*, Structural and functional studies of Bud23-Trm112 reveal 18S rRNA N7–G1575 methylation occurs on late 40S precursor ribosomes. *Proc. Natl. Acad. Sci. U.S.A.* **111**, E5518–E5526 (2014).
22. M. Charette, M. W. Gray, Pseudouridine in RNA: What, where, how, and why. *IUBMB Life* **49**, 341–351 (2000).
23. J. Y. Hahm, J. Park, E. S. Jang, S. W. Chi, 8-Oxoguanine: From oxidative damage to epigenetic and epitranscriptional modification. *Exp. Mol. Med.* **54**, 1626–1642 (2022).
24. H. Hao *et al.*, N6-methyladenosine modification and METTL3 modulate enterovirus 71 replication. *Nucleic Acids Res.* **47**, 362–374 (2019).
25. A. M. Price *et al.*, Direct RNA sequencing reveals m(6)A modifications on adenovirus RNA are necessary for efficient splicing. *Nat. Commun.* **11**, 6016–19787 (2020).
26. B. A. Henry *et al.*, 5-methylcytosine modification of an Epstein-Barr virus noncoding RNA decreases its stability. *RNA* **26**, 1038–1048 (2020).
27. Y. Wang *et al.*, N(6)-methyladenosine in 7SK small nuclear RNA underlies RNA polymerase II transcription regulation. *Mol. Cell.* **83**, 3818–3834 (2023).
28. E. Sendinc, Y. Shi, RNA m6A methylation across the transcriptome. *Mol. Cell.* **83**, 428–441 (2023).
29. Y. Xiang *et al.*, RNA m(6)A methylation regulates the ultraviolet-induced DNA damage response. *Nature* **543**, 573–576 (2017).
30. X. Deng *et al.*, DNA damage signaling is required for replication of human bocavirus 1 DNA in dividing HEK293 cells. *J. Virol.* **91**, e01831-16 (2016).
31. X. Deng *et al.*, Replication of an autonomous human parvovirus in non-dividing human airway epithelium is facilitated through the DNA damage and repair pathways. *PLoS Pathog.* **12**, e1005399 (2016).
32. P. Tijerina, S. Mohr, R. Russell, DMS footprinting of structured RNAs and RNA–protein complexes. *Nat. Protoc.* **2**, 2608–2623 (2007).
33. M. Zubradt *et al.*, DMS-MaPseq for genome-wide or targeted RNA structure probing in vivo. *Nat. Methods* **14**, 75–82 (2017).
34. J. Zhao *et al.*, The RNA architecture of the SARS-CoV-2 3′-untranslated region. *Viruses* **12**, 1473 (2020).
35. S. Busan, K. M. Weeks, Accurate detection of chemical modifications in RNA by mutational profiling (MaP) with ShapeMapper 2. *RNA* **24**, 143–148 (2018).
36. M. J. Smola *et al.*, Selective 2′-hydroxyl acylation analyzed by primer extension and mutational profiling (SHAPE-MaP) for direct, versatile and accurate RNA structure analysis. *Nat. Protoc.* **10**, 1643–1669 (2015).
37. K. M. Schoch, T. M. Miller, Antisense oligonucleotides: Translation from mouse models to human neurodegenerative diseases. *Neuron.* **94**, 1056–1070 (2017).
38. R. Giegé, J. D. Puglisi, C. Florentz, tRNA structure and aminoacylation efficiency. *Prog. Nucleic Acid Res. Mol. Biol.* **45**, 129–206 (1993).
39. T. Suzuki, The expanding world of tRNA modifications and their disease relevance. *Nat. Rev. Mol. Cell Biol.* **22**, 375–392 (2021).
40. D. L. Balacco, M. Soller, The m(6)A writer: Rise of a machine for growing tasks. *Biochemistry* **58**, 363–378 (2019).
41. C. J. Lewis, T. Pan, A. Kalsotra, RNA modifications and structures cooperate to guide RNA–protein interactions. *Nat. Rev. Mol. Cell Biol.* **18**, 202–210 (2017).
42. K. D. Meyer, S. R. Jaffrey, Rethinking m(6)A readers, writers, and erasers. *Annu. Rev. Cell Dev. Biol.* **33**, 319–342 (2017).
43. M. Xue *et al.*, Viral N(6)-methyladenosine upregulates replication and pathogenesis of human respiratory syncytial virus. *Nat. Commun.* **10**, 4595–12504 (2019).
44. Y. Yue, J. Liu, C. He, RNA N6-methyladenosine methylation in post-transcriptional gene expression regulation. *Genes Dev.* **29**, 1343–1355 (2015).
45. Y. Zhou *et al.*, SRAMP: Prediction of mammalian N6-methyladenosine (m6A) sites based on sequence-derived features. *Nucleic Acids Res.* **44**, e91 (2016).
46. M. Zuker, Mfold web server for nucleic acid folding and hybridization prediction. *Nucleic Acids Res.* **31**, 3406–3415 (2003).
47. A. Xayaphoummine, T. Bucher, H. Isambert, Kinefold web server for RNA/DNA folding path and structure prediction including pseudoknots and knots. *Nucleic Acids Res.* **33**, W605–W610 (2005).
48. P. C. He, C. He, m(6) A RNA methylation: From mechanisms to therapeutic potential. *EMBO J.* **40**, e105977 (2021).
49. R. Dijkman *et al.*, Human bocavirus can be cultured in differentiated human airway epithelial cells. *J. Virol.* **83**, 7739–7748 (2009).
50. J. Zabner *et al.*, Development of cystic fibrosis and noncystic fibrosis airway cell lines. *Am. J. Physiol. Lung. Cell Mol. Physiol.* **284**, L844–L854 (2003).
51. J. D. Thompson, T. J. Gibson, D. G. Higgins, Multiple sequence alignment using ClustalW and ClustalX. *Curr. Protoc. Bioinf.* **Chapter 2**, Unit 2.3 (2002).
52. L. Shao, W. Shen, S. Wang, J. Qiu, Recent advances in molecular biology of human bocavirus 1 and its applications. *Front. Microbiol.* **12**, 696604 (2021).
53. X. Wang *et al.*, N6-methyladenosine-dependent regulation of messenger RNA stability. *Nature* **505**, 117–120 (2014).
54. X. Wang *et al.*, N(6)-methyladenosine modulates messenger RNA translation efficiency. *Cell* **161**, 1388–1399 (2015).
55. A. S. Warda *et al.*, Human METTL16 is a N(6)-methyladenosine (m(6)A) methyltransferase that targets pre-mRNAs and various non-coding RNAs. *EMBO Rep.* **18**, 2004–2014 (2017).
56. X. Yang *et al.*, m(6)A promotes R-loop formation to facilitate transcription termination. *Cell Res.* **29**, 1035–1038 (2019).
57. J. M. Santos-Pereira, A. Aguilera, R loops: New modulators of genome dynamics and function. *Nat. Rev. Genet.* **16**, 583–597 (2015).
58. S. F. Cotmore, P. Tattersall, Parvoviruses: Small does not mean simple. *Annu. Rev. Virol.* **1**, 517–537 (2014).
59. Y. Yang *et al.*, Structural basis of RNA conformational switching in the transcriptional regulator 7SK RNP. *Mol. Cell.* **82**, 1724–1736 (2022).
60. S. W. Olson *et al.*, Discovery of a large-scale, cell-state-responsive allosteric switch in the 7SK RNA using DANCE-MaP. *Mol. Cell.* **82**, 1708–1723 (2022).
61. J. Wang, Data from "DMS-MaPseq of BocaSR RNA in Human Bocavirus 1 (HBoV1)". NCBI Bioproject PRJN955716. https://www.ncbi.nlm.nih.gov/bioproject/955716. Deposited 14 April 2023.